Check for updates

View Article Online
View Journal

PCCP
Physical Chemistry Chemical Physics

Accepted Manuscript

This article can be cited before page numbers have been issued, to do this please use: Z. Xie, S. Gao, X. Ye, H. Yang, G. Gong, Y. Lu, J. Ye, G. Liu and R. Li, *Phys. Chem. Chem. Phys.*, 2020, DOI: 10.1039/D0CP03767B.

This is an Accepted Manuscript, which has been through the Royal Society of Chemistry peer review process and has been accepted for publication.

Accepted Manuscripts are published online shortly after acceptance, before technical editing, formatting and proof reading. Using this free service, authors can make their results available to the community, in citable form, before we publish the edited article. We will replace this Accepted Manuscript with the edited and formatted Advance Article as soon as it is available.

You can find more information about Accepted Manuscripts in the Information for Authors.

Please note that technical editing may introduce minor changes to the text and/or graphics, which may alter content. The journal's standard Terms & Conditions and the Ethical guidelines still apply. In no event shall the Royal Society of Chemistry be held responsible for any errors or omissions in this Accepted Manuscript or any consequences arising from the use of any information it contains.

View Article Online
DOI: 10.1039/D0CP03767B

Magnetism Modulation and Conductance Quantization in a Gadolinium Oxide Memristor

Zhuolin Xie,[ab] Shuang Gao,*[a] Xiaoyu Ye,[ab] Huali Yang,[a] Guodong Gong,[ab] Ying Lu,[ab] Junya Ye,[ab] Gang Liu,[c] Run-Wei Li*[a]

[a] CAS Key Laboratory of Magnetic Materials and Devices, and Zhejiang Province Key Laboratory of Magnetic Materials and Application Technology, Ningbo Institute of Materials Technology and Engineering, Chinese Academy of Sciences, Ningbo 315201, China. E-mail: gaoshuang@nimte.ac.cn, runweili@nimte.ac.cn

[b] College of Materials Sciences and Opto-Electronic Technology, University of Chinese Academy of Sciences, Beijing 100049, China

[c] School of Electronic Information and Electrical Engineering, Shanghai Jiao Tong University, Shanghai 200240, China.

Published on 31 October 2020. Downloaded on 11/1/2020 7:31:47 AM.

Physical Chemistry Chemical Physics Accepted Manuscript

View Article Online
DOI: 10.1039/D0CP03767B

Abstract: The requests for higher information storage density, greater data processing power and memory-centric computing capability in the current big data era are motivating global research interests on novel solid-state electronic devices that can unite the electron charge and spin degrees of freedom. Herein, simultaneous realization of magnetism modulation and conductance quantization in a single gadolinium oxide memristor is reported. A remarkable enhancement of >170% in saturation magnetization at room temperature, accompanied by the emergence of a clear magnetoresistance behavior at low temperature, is obtained after setting the memristor from the initial high resistance state (HRS) into the low resistance state (LRS). By carefully resetting the memristor from the LRS into the HRS, up to 32 quantized conductance states with good repeatability and stability are observed, which is possible for achieving 5 bit storage in a single memory cell in future. Moreover, resistive switching mechanism of the memristor has been thoroughly discussed with the help of temperature-dependent resistance test and high-resolution transmission electron microscopy examination. This work could provide a powerful approach to design future multi-field modulated, high-performance information devices with integrated data storage, sensing as well as processing functions.

Keywords: memristor, resistive switching, magnetism modulation, conductance quantization, gadolinium oxide

Published on 31 October 2020. Downloaded on 11/1/2020 7:31:47 AM.

Physical Chemistry Chemical Physics Accepted Manuscript

View Article Online
DOI: 10.1039/D0CP03767B

1. Introduction

Charge and spin are two inherent properties of electrons. Along with the ever increasing understanding about the physics and manipulation techniques of electron charges in semiconductors over the past 70 years, an astounding revolution based on the miniaturization campaign of transistor devices has surged globally in the microelectronic industry, which follows the prediction of Moore's Law to continuously refresh the complexity and performance of modern integrated circuits. However, as the feature size of the charge-based semiconductor devices shrinks to less than 10 nm, issues including quantum uncertainty, power consumption, heat death and production cost arise steadily, making the Moore's Law no longer sustainable in the foreseeable future.[1-2] Developing new-principle information devices that are qualified for the data-intensive tasks in the current big data and artificial intelligence era thus appears increasingly urgent.

Memristor is such a newly found memory device working on ions rather than electrons to store the digital data, with versatile features of simple "metal/insulator/metal" sandwich-like device structure, fast operating speed, good CMOS compatibility and high-density integration through crossbar arrays.[3-7] The electric field-induced migration and redox reaction of the ionic species can lead to the precipitation and growth of conducting filaments (CFs) for easy electron transport inside the insulating matrix, the reversible annihilation and re-formation of which alternately switch the device between a high resistance state (HRS or OFF state) and a low resistance state (LRS or ON state). Due to the mass of ions/atoms much larger than that of electrons, the as-formed CFs are robust and the resistive switching characteristics of the memristors are non-volatile in nature, thus eliminating the power consumption required to

Published on 31 October 2020. Downloaded on 11/1/2020 7:31:47 AM.

Physical Chemistry Chemical Physics Accepted Manuscript

View Article Online
DOI: 10.1039/D0CP03767B

constantly maintain the stored data and overcoming the miniaturization limit of conventional charge-based memory devices.[8-9] More importantly, when the lateral dimension of the CFs (in particular the diameter of the narrowest region) is approaching the atomic scale, atomic point contacts (APCs) with conductance quantized in the unit of $2e^2/h$ (where e is the charge of electron and h is the Planck constant) will be generated.[10-14] The conductance quantization feature not only extends the life time of Moore's Law through ultra-small memristor devices, but offers the possibility of developing quantum and neuromorphic information technique for memory-centric computing paradigms.

As the other inherent property of electrons, spin can also be used to modulate electron transport for the construction of data storage and memory devices that have dimensions of just a few nanometers,[15-18] a size scale at which conventional charge-based semiconductor gadgets face enormous challenges. Interestingly, researchers have recently demonstrated that by utilizing magnetic metals like Ni and Co as the electrochemically active electrode to generate magnetic CFs in memristors, magnetism modulation with the emergence of various magnetoresistance (MR) behaviors such as anisotropic and tunneling MR (AMR and TMR) can be achieved for potential multi-level magneto-electric coupling storage and sensor-in-memory applications.[19-22] In case that we can well marry the spin and charge degrees of freedom of the CFs in a single memristor, it may introduce more exotic solid-state physical phenomena and broaden device applications. Nevertheless, its realization requires systematic optimization on both the active switching materials and operation mechanisms of memristors.

In this contribution, we report the simultaneous realization of magnetism modulation and

Published on 31 October 2020. Downloaded on 11/1/2020 7:31:47 AM.

Physical Chemistry Chemical Physics Accepted Manuscript

View Article Online
DOI: 10.1039/D0CP03767B

conductance quantization in a single gadolinium oxide (Gd_2O_3) memristor. The successful construction of magnetic Gd CFs *via* electric field-induced migration of oxygen ions has been definitely confirmed by temperature-dependent resistance test and high-resolution transmission electron microscopy (HRTEM) examination. Due to the formation of such CFs, a remarkable enhancement of >170% in saturation magnetization at room temperature, accompanied by the emergence of a clear MR behavior at low temperature, has been observed when the memristor was set from the initial HRS into the LRS. Meanwhile, through precisely modulating the lateral dimension of Gd CFs during the reset process, up to 32 quantized conductance states with good repeatability and stability have been observed in the present memristor. These results could help to develop high-performance multi-field modulated information storage as well as processing devices in future.

2. Experimental

Sample preparation. A 10 nm thick Gd_2O_3 film was firstly deposited on the commercial indium tin oxide (ITO)-coated glass substrate by radio-frequency (RF) magnetron sputtering (JGP450, SKY Technology CAS) at room temperature. The base vacuum of sputtering chamber was lower than 2×10^{-4} Pa. A high-purity (99.99%) Gd_2O_3 ceramic with the diameter of 2 inch and thickness of 3 mm was used as the sputtering target. During sputtering, high-purity (99.999%) mixture gas of Ar and O_2 with the ratio of 4:1 and total pressure of 0.9 Pa was introduced into the chamber, while the RF power was fixed to be 60 W. Subsequently, isolated Pt top electrodes (TEs) with the thickness of 30 nm were deposited by electron beam evaporation (ULVAC, MUE-ECO) with the help of shadow masks with circular holes of 150 or 300 μm in diameter, resulting in the final memristor structure of Pt/Gd_2O_3/ITO. Besides, to

Published on 31 October 2020. Downloaded on 11/1/2020 7:31:47 AM.

Physical Chemistry Chemical Physics Accepted Manuscript

View Article Online
DOI: 10.1039/D0CP03767B

enable standard four-terminal MR measurement, crosspoint-type Pt/Gd_2O_3/Pt memristors with an effective cell area of 100 × 100 μm^2 were also fabricated. Herein, the Pt bottom electrode (BE) strips were designed to be 30 nm in thickness and patterned by shadow mask, whereas their top counterparts with the thickness of 30 nm were patterned by conventional ultraviolet lithography and lift-off processes. For the Gd_2O_3 film, it was optimized to be 13 nm in thickness to guarantee good insulation.

Sample characterization. Crystalline structure of the as-deposited Gd_2O_3 film was investigated by X-ray diffraction (XRD, D8 Discover, Bruker AXS) using Cu-Kα radiation. Scanning probe microscopy (SPM, Dimension 3100V, Veeco) was employed for film morphology and conductivity measurements. Microstructures of the memristors in different resistance states were characterized by HRTEM (Titan Themis 200, FEI) with corresponding cross-sectional specimens prepared on a dual-beam focus ion beam (FIB) workstation (Helios 450S, FEI). All resistive switching-related electrical measurements were conducted on a Lakeshore probe station with a Keithley 4200 semiconductor parameter analyzer in the atmosphere and at room temperature. External voltages were always applied onto the Pt TE with the ITO or Pt BE grounded. Magnetic hysteresis loops were obtained in a superconducting quantum interference device (SQUID, Quantum Design) magnetometer with in-plane magnetic fields (parallel to the sample surface) at room temperature, whereas MR characteristics were measured by a self-built magneto-electronic transport measurement system with low temperature down to 1.2 K and high magnetic field up to 12 T. Temperature-dependent resistance test was implemented using a physical property measurement system (PPMS, Quantum Design).

Published on 31 October 2020. Downloaded on 11/1/2020 7:31:47 AM.

Physical Chemistry Chemical Physics Accepted Manuscript

View Article Online
DOI: 10.1039/D0CP03767B

3. Results and discussion

Fig. 1a shows the schematic of the sample layout and measurement configuration. The active switching layer was selected to be Gd_2O_3 due to the following reasons. First, Gd_2O_3 has been demonstrated to be a promising resistive switching material with high resistivity, easy deposition, large energy gap, high dielectric permittivity and good thermodynamic stability.[23] Next, Gd is a ferromagnetic metallic element with Curie point around room temperature, which could establish the foundation for remarkable magnetism modulation through resistive switching.[24] Finally, unlike the oxides of other common ferromagnetic metallic elements (for example, NiO and CoO) showing mostly unipolar resistive switching with the thermochemical mechanism,[25-26] Gd_2O_3 has been found to prefer bipolar resistive switching due to the oxygen ion migration mechanism,[23,27,28] thus being well-suited for realizing conductance quantization[12,29,30]. As for electrode materials, Pt and ITO were adopted because of their good electrochemically inert property so that our memristors are operated indeed based on the expected oxygen ion migration mechanism.

Prior to resistive switching measurement, microstructure analysis was firstly conducted on the fabricated Pt/Gd_2O_3/ITO memristor. Fig. 1b shows a cross-sectional HRTEM image of the memristor structure. One can see clear top Pt/Gd_2O_3 and bottom Gd_2O_3/ITO interfaces, indicating that the deposited Gd_2O_3 film is dense and free of elements inter-diffusion with the electrode materials. The inset of this figure is the magnified lattice fringe image of one typical Gd_2O_3 crystalline grain, which reveals a *d*-spacing of ~0.31 nm. On the other hand, XRD pattern of the Gd_2O_3 film exhibits a dominating peak at 2θ of ~28.3°, as shown in Fig. 1c. The two features agree well with each other, demonstrating that the deposited Gd_2O_3 film has a

Published on 31 October 2020. Downloaded on 11/1/2020 7:31:47 AM.

Physical Chemistry Chemical Physics Accepted Manuscript

View Article Online
DOI: 10.1039/D0CP03767B

polycrystalline cubic phase.[31] It is noted herein that a pure glass substrate, rather than an ITO-coated glass substrate, was used for the XRD analysis in Fig. 1c. This is because the weak diffraction peaks of the Gd_2O_3 film can be submerged by the strong diffraction peaks of the high-crystallinity ITO electrode layer (Fig. S1). Besides, SPM analysis suggests that the Gd_2O_3 film not only has a smooth surface topography (Fig. S2) but also is uniform in electrical insulation (Fig. 1d), both of which are beneficial for memristor applications.

Published on 31 October 2020. Downloaded on 11/1/2020 7:31:47 AM.

With the measurement configuration in Fig. 1a, resistive switching performance of the Pt/Gd_2O_3/ITO memristor had been carefully studied. The as-fabricated device had a high resistance of ~10^4 Ω. During the first voltage sweeping from 0 to 2 V, the device current was found to gradually increase in the low voltage region and then abruptly jump from ~100 μA to the compliance current of 1 mA at ~0.8 V, as shown by the blue current–voltage (*I–V*) curve in Fig. 2a. This indicates that the device had been set from the initial HRS into the LRS, and can be well explained by the formation of local CFs in the Gd_2O_3 film due to electric field-driven outward migration of oxygen ions from the oxide film. The bubbles formed between the Pt TE and the oxide film after device operation are strong evidence for the migration of oxygen ions (Fig. S3). The LRS had a resistance of ~300 Ω and thus resulted in a high memory window of >10. Also, the LRS was nonvolatile in nature, as evidenced by the high current during the subsequent backward voltage sweeping. To reset the device back into the HRS, a negative voltage sweeping was necessary and the device current started to decrease at ~–0.4 V. Such process can be attributed to the gradual annihilation of already existing CFs through backward migration of oxygen ions into the Gd_2O_3 film. Since set and reset processes were completed under opposite voltage polarities, the device indeed exhibited

Physical Chemistry Chemical Physics Accepted Manuscript

View Article Online
DOI: 10.1039/D0CP03767B

a bipolar resistive switching behavior, as expected based on our device structure design. The device was able to be consecutively operated for more than 60 cycles without apparent degradation in memory window (Fig. S4a,b), which could be greatly improved by interface engineering, such as introducing an interfacial sub-oxide layer,[32] in our future work. The operation voltage distributions are very tight with V_{set} from 0.8 to 1.0 V and V_{reset} from –0.6 to –0.3 V (Fig. 2b). Notably, the V_{set} values for the first and second operation cycles were almost equal (Fig. 2a), demonstrating actually a forming-free resistive switching behavior that is beneficial for practical applications.[33] Also, response speed of the device has been evaluated by the pulse operation mode, revealing a fast switching speed of no larger than 100 ns for both set and reset operations (Fig. S4c,d). Moreover, both HRS and LRS were found to remain unchanged for at least 10^6 s (Fig. 2c), thus confirming a fairly good nonvolatile memory effect in the present memristor.

To clarify the detailed composition of the formed CFs in the Pt/Gd_2O_3/ITO memristor, both temperature-dependent resistance test and cross-sectional HRTEM examination had been conducted on the LRS device. As shown in Fig. 2d, the resistance of the LRS device was found to decrease almost linearly with temperature in a wide range of 100 to 300 K, indicating a typical metallic conduction behavior. Further, quantitative calculation revealed a temperature coefficient of resistance (α) of 1.21×10^{-3} K^{-1} at 300 K, which is similar to that of metallic nanowires with a nanoscale diameter.[34-35] The two points both imply that the formed CFs should be mainly composed of metallic Gd atoms. Fig. 2e displays a representative cross-sectional HRTEM image of the LRS device, from which one can clearly see a nanochannel region with distinct crystallographic features from the surrounding Gd_2O_3

Published on 31 October 2020. Downloaded on 11/1/2020 7:31:47 AM.

Physical Chemistry Chemical Physics Accepted Manuscript

View Article Online
DOI: 10.1039/D0CP03767B

regions. As outlined by the dotted white lines, the Pt and ITO electrodes are directly connected by the nanochannel region with its wider and narrower ends at the Pt/Gd_2O_3 and Gd_2O_3/ITO interfaces, respectively. More importantly, a smaller *d*-spacing of ~0.2 nm can be definitely observed in such nanochannel region (Fig. 2e-2 and 2e-3), which corresponds well to the (102) crystal plane of Gd metal.[31] In combination of these results, we can definitely conclude that it is the formation of metallic Gd CFs that causes the memristor to be switched from HRS into LRS.

Considering that Gd is a ferromagnetic metallic element with Curie point around room temperature, apparent magnetism modulation can be naturally expected in the Pt/Gd_2O_3/ITO memristor along with the reversible formation and annihilation processes of the Gd CFs in it. To confirm this point, a 3 × 5 mm^2 sample with multiple Pt electrodes of 300 μm in diameter was intentionally fabricated and carefully examined by SQUID with in-plane magnetic field (*H*) at room temperature, as schematically shown in Fig. 3a. It is noted that the diameter of Pt electrodes had been increased from 150 μm for normal resistive switching measurement to 300 μm herein to magnify magnetic signals, resulting in a total coverage ratio of ~33% for Pt electrodes. Fig. 3b shows the magnetization hysteresis loops of the sample with the memristors in various resistance states, where the diamagnetic signal of the substrate has already been subtracted for accuracy. For the pristine sample, only a small saturation magnetization (M_s) of ~49 emu/cm^3 was observed, which can be reasonably attributed to the potential d^0 ferromagnetism that originating from lattice defects.[36-37] In sharp contrast, a very high M_s of ~137 emu/cm^3 was obtained after all the memristors were set into LRS, which corresponds to a huge increase ratio of >170% and should be contributed mainly by the

Published on 31 October 2020. Downloaded on 11/1/2020 7:31:47 AM.

Physical Chemistry Chemical Physics Accepted Manuscript

View Article Online
DOI: 10.1039/D0CP03767B

formed Gd CFs. Such value is also among the highest level when compared to that in previous works.[17,38-41] Subsequently, after the existing Gd CFs were annihilated by resetting the memristors into HRS, the M_s was found to decrease accordingly to ~90 emu/cm^3. Such resistive switching-induced magnetism modulation phenomenon was robust and had been repeated for several times (Fig. 3c), thus holding the potential for future novel applications such as multi-level magneto-electric coupling storage. The relatively higher M_s for the HRS sample than its pristine counterpart can be readily understood in terms of the complete formation of Gd CFs during the first set operation and their partial annihilation and re-formation in the subsequent resistive switching operations.[18,41,42]

Besides magnetism modulation, the spin degree of freedom of the Gd CFs has also been evaluated through careful MR measurements. Herein, crosspoint-type Pt/Gd_2O_3/Pt memristors with an effective cell area of 100 × 100 μm^2 were used to enable the standard four-terminal MR measurement with in-plane magnetic field, as schematically shown in Fig. 3d. It is noted that the substitution of the Pt BE for the ITO BE was mainly for easy device patterning and had little influence on the resistive switching behavior (Fig. S5). Representative MR curves of the LRS and HRS devices measured at 2 K with the in-plane magnetic field are shown in Fig. 3e and 3f, respectively. For the LRS device, one can see a low resistance of ~146.2 Ω at zero field due to the formation of complete Gd CFs in it.[41-42] Importantly, the device resistance gradually increases with H and becomes saturated to be ~148.6 Ω at H of ~3 kOe, resulting in a credible MR value of ~1.64%. Previous works have demonstrated that the appearance of MR in a LRS memristor can be a convincing support for the formation of ferromagnetic CFs.[18,41,42] It is therefore concluded that the spin degree of freedom has indeed been

Published on 31 October 2020. Downloaded on 11/1/2020 7:31:47 AM.

Physical Chemistry Chemical Physics Accepted Manuscript

View Article Online
DOI: 10.1039/D0CP03767B

introduced into the Gd CFs. Based on this scenario, no MR behavior should be observed in the HRS device due to the annihilation of ferromagnetic Gd CFs, according well with the data in Fig. 3f. It is mentioned that no MR behavior was observed for the LRS device around room temperature (300K), which may result from the Curie point reduction phenomenon due to small size effect.[43] Meanwhile, low-temperature measurements can significantly reduce the impact of environmental and thermal disturbances, thus making the relatively weak magneto-electronic transport property to be more readily observed. Even so, the involvement of MR behavior into the present memristor could make it suitable for future sensor-in-memory applications.

Finally, the attention is paid to the size-dependent electron transport features of the Gd CFs in the Pt/Gd_2O_3/ITO memristor. Previous works have suggested that the CFs in memristors can be treated as APCs when their lateral dimension (in particular the diameter of the narrowest region) is approaching the atomic scale. In this case, the conductance of CFs will be mainly determined by the size of the APC restrictions and thus quantized in the unit of $G_0 = 2e^2/h = \sim 77.5$ μS. Since the CFs are the primary contributions to the electrical properties of a LRS memristor, the size-dependent electron transport features of Gd CFs can therefore be well linked to the conductance quantization effect of the Pt/Gd_2O_3/ITO memristor. Experimentally, conductance quantization effect of the present memristor has been examined in detail during the reset process because the gradual decrease in device current during such process has been proved to be more favorable for CFs size modulation.[13,29]

Fig. 4a shows a representative reset process of the Pt/Gd_2O_3/ITO memristor in the conductance–voltage (G–V) plot, where the step increment for voltage sweeping was

Published on 31 October 2020. Downloaded on 11/1/2020 7:31:47 AM.

Physical Chemistry Chemical Physics Accepted Manuscript

View Article Online
DOI: 10.1039/D0CP03767B

intentionally reduced to 0.01 V to reveal more details. One can see the appearance of clear quantized conductance plateaus at around $13G_0$, $11G_0$, $10G_0$, $9G_0$, $8G_0$, $6G_0$, $4G_0$ and $1G_0$ in sequence. This phenomenon can be a solid evidence for conductance quantization and also suggests the possibility of constructing Gd CFs with various lateral dimensions by utilizing different stop voltages during the reset process. As confirmed in Fig. 4b and S6, the device conductance has indeed been programmed into a serious of discrete quantized values by gradually changing the stop voltage for reset process from –0.5 to –1 V with the increment of –0.05 V. It is noted that besides the common quantized values of integer multiples of G_0, those of half-integer multiples of G_0 have also been observed, such as the $7.5G_0$, $5.5G_0$ and $3.5G_0$ for the stop voltages of –0.55, –0.65 and –0.75 V, respectively. Statistical analysis on quantized conductance values has been further made based on 1376 reset traces, as displayed by the histogram with a counting step of $0.1G_0$ in Fig. 4c. Discrete conductance peaks, locating definitely at both integer and half-integer multiples of G_0 in the range of $0.5G_0$ to $16G_0$, dominate the histogram. In sharp contrast, previous conductance histograms for the memristors with non-magnetic metallic Ag or Cu CFs tend to have peaks merely at integer multiples of G_0.[12] Such difference can be another fair indicator for the formation of spin-polarized Gd CFs in the present memristor because the spin splitting has been acknowledged as the common origin of half-integer conductance quantization in metallic APCs.[14,44,45] More importantly, the combination of integer and half-integer conductance quantization effects into a single memristor is highly beneficial for ultra-high-density data storage applications. Specifically, the observed 32 quantized conductance states due to the size-dependent electron transport features of Gd CFs could enable the $Pt/Gd_2O_3/ITO$

Published on 31 October 2020. Downloaded on 11/1/2020 7:31:47 AM.

Physical Chemistry Chemical Physics Accepted Manuscript

View Article Online
DOI: 10.1039/D0CP03767B

memristor to store 5 bit in a single cell in future, which is four times higher than that for ordinary memristors with only 1 bit per cell. Moreover, these quantized conductance states have been confirmed to be highly repeatable and stable (Fig. 4d and 4e), thus holding a great potential for future high-performance data storage as well as processing applications. Nevertheless, the modulation accuracy of conductance quantization is still needed to be further improved in our future works, especially given the notable device-to-device variability of common memristors. This has also been acknowledged as one of the key challenges in such research field.[12]

4. Conclusions

In summary, magnetism modulation and conductance quantization are simultaneously realized in the Pt/Gd_2O_3/ITO memristor. The memristor shows basically a forming-free bipolar resistive switching behavior with high memory window of >10 and good data retention of >10^4 s. By combining temperature-dependent resistance test and HRTEM examination, resistive switching mechanism of the memristor is attributed to the reversible formation and annihilation of magnetic Gd CFs *via* electric field-induced migration of oxygen ions. Due to the formation of such CFs, a remarkable enhancement of >170% in saturation magnetization at room temperature, accompanied by the emergence of a clear MR of ~1.64% at 2 K, is observed after setting the memristor from the initial HRS into the LRS. Meanwhile, through precisely modulating the lateral dimension of Gd CFs during the reset process, up to 32 quantized conductance states with good repeatability and stability have been observed in the memristor, which is possible for achieving 5 bit storage in a single memory cell in future. These results could help to develop future multi-field modulated, high-performance

Published on 31 October 2020. Downloaded on 11/1/2020 7:31:47 AM.

Physical Chemistry Chemical Physics Accepted Manuscript

View Article Online
DOI: 10.1039/D0CP03767B

information storage as well as processing devices.

Conflicts of interest

The authors declare no conflicts of interest.

Acknowledgements

This work was supported by the National Key R&D Program of China (2017YFB0405604), National Natural Science Foundation of China (61974179, 61841404, 61704178, 61774161, 51525103, 61674153, 61722407 and 51931011), Youth Innovation Promotion Association of the CAS (2020297), and Natural Science Foundation of Zhejiang Province (LR17E020001).

References

1. D. S. Jeong, K. M. Kim, S. Kim, B. J. Choi and C. S. Hwang, *Adv. Electron. Mater., 2016,* **2**, 1-27.
2. H. N. Khan, D. A. Hounshell and E. R. H. Fuchs, *Nat. Electron.*, 2018, **1**, 14-21.
3. J. J. Yang, D. B. Strukov and D. R. Stewart, *Nat. Nanotechnol.*, 2013, **8**, 13-24.
4. X. J. Zhu, S. H. Lee and W. D. Lu, *Adv. Electron. Mater.*, 2019, **5**, 1900184.
5. S. Pi, C. Li, H. Jiang, W. W. Xia, H. L. Xin, J. J. Yang and Q. F. Xia, *Nat. Nanotechnol.*, 2019, **14**, 35-40.
6. F. Pan, S. Gao, C. Chen, C. Song and F. Zeng, *Mater. Sci. Eng. R Rep.*, 2014, **83**, 1-59.
7. I. Valov, *Nature Electron.*, 2019, **2**, 56-57.
8. T. C. Chang, K. C. Chang, T. M. Tsai, T. J. Chu and S. M. Sze, *Mater. Today*, 2015, **19**, 254-264.
9. N. Xiao, M. A. Villena, B. Yuan, S. C. Chen, B. R. Wang, M. Eliáš, Y. Y. Shi, F. Hui, X. Jing, A. Scheuerman, K. Tang, P. C. McIntyre and M. Lanza, *Adv. Funct. Mater.*, 2017, **27**, 1700384.
10. K. Terabe, T. Hasegawa, T. Nakayama and M. Aono, *Nature*, 2005, **433**, 47-50.
11. W. Yi, S. E. Savel'ev, G. M. Ribeiro, F. Miao, M. X. Zhang, J. J. Yang, A. M. Bratkovsky and R. S. Williams, *Nat. Commun.*, 2016, **7**, 11142.
12. W. H. Xue, S. Gao, J. Shang, X. H. Yi, G. Liu and R. W. Li, *Adv. Electron. Mater.*, 2019, **5**, 1800854.
13. K. Krishnan, M. Muruganathan, T. Tsuruoka and H. Mizuta, *Adv. Funct. Mater.*, 2017,**27**, 1605104 .
14. B. C. Jang, S. Kim, S. Y. Yang, J. Park, J. H. Cha, J. Oh, J. Choi, S. G. Im, V. P. Dravid and S. Y. Choi, Hwang *Nano Lett.*, 2019, **19**, 2, 839-849.

Published on 31 October 2020. Downloaded on 11/1/2020 7:31:47 AM.

Physical Chemistry Chemical Physics Accepted Manuscript

View Article Online
DOI: 10.1039/D0CP03767B

15. S. A. Wolf, D. D. Awschalom, R. A. Buhrman, J. M. Daughton, S. V. MoLn'r, M. L. Roukes, A. Y. Chtchelkanova and D. M. Treger, *Science*, 2016, **294**, 1488-1495.
16. X. J. Zhu, J. T. Zhou, L. Chen, S. S. Guo, G. Liu, R. W. Li and W. D. Lu, *Adv. Mater.*, 2016, **28**, 7658-7665.
17. G. Chen, C. Song, C. Chen, S. Gao, F. Zeng and F. Pan, *Adv. Mater.*, 2012, **24**, 3515.
18. L. F. Wang, X. L. Li, W. H. Xue, Z.Y. Quan, X. F. Qin, F. Wang and X. H. Xu, *J. Mater. Chem. C*, 2018, **6**, 1996-2003.
19. L. L. Li, Y. Liu, J. Teng, S. B. Long, Q. X. Guo, M. Y. Zhang, Y. Wu, G. H. Yu, Q. Liu, H. B. Lv and M. Liu, *Nanoscale Res. Lett.*, 2017, **12**, 10-15.
20. S. Otsuka, Y. Hamada, D. Ito, T. Shimizu and S. Shingubara, *Jpn. J. Appl. Phys.*, 2014, **54**, 05ED02.
21. S. Otsuka, Y. Hamada, T. Shimizu and S. Shingubara, *Appl. Phys. A*, 2015, **118**, 613-619.
22. Z. H. Yang, Q. F. Zhan, X. J. Zhu, Y. W. Liu, H. L. Yang, B. L. Hu, J. Shang, L. Pan, B. Chen and R. W. Li, *Europhys. Lett.*, 2014, **108**, 58004.
23. D. Jana, S. Maikap, A. Prakash, Y. Y. Chen, H. C. Chiu and J. R. Yang, *Nanoscale Res. Lett.*, 2014, **9**, 12.
24. Q. L. Chen, G. Liu, S. Gao, X. H. Yi, W. H. Xue, M. H. Tang, X. J. Zheng and R. W. Li, *MRS Commun.*, 2019, **9**, 14-26.
25. B. K. You, W. I. Park, J. M. Kim, K. Park, H. K. Seo, J. Y. Lee, Y. S. Jung and K. J. Lee. *ACS Nano*, 2014, **8**, 9492-9502.
26. Z. Q. Wang, X. H. Li, H. Y. Xu, W. Wang, H. Yu, X. T. Zhang, Y. X. Liu and Y. C. Liu, *J. Phys. D: Appl. Phys.*, 2010, **43**, 385105.
27. Q. G. Zhou and J. W. Zhai, *Phys. Status Solidi A*, 2014, **211**, 173-179.
28. C. Sun, S. M. Lu, F. Jin, W. Q. Mo, J. L. Song and K. F. Dong, *J. Alloys Compd.*, 2019, **816**, 152564.
29. W. H. Xue, Y. Li, G. Liu, Z. R. Wang, W. Xiao, K. M. Jiang, Z. C. Zhong, S. Gao, J. Ding, X. S. Miao, X. H. Xu and R. W. Li, *Adv. Electron. Mater.*, 2019, **6**, 1901055.
30. S. U. Sharath, S. Vogel, L. M. Luna, E. Hildebrandt, C. Wenger, J. Kurian, M. Duerrschnabel, T. Niermann, G. Niu, P. Calka, M. Lehmann, H. J. Kleebe, T. Schroeder and L. Alff, *Adv. Funct. Mater.*, 2017, **27**, 1700432.
31. X. Cao, X. M. Li, X. D. Gao, W. D. Yu, X. J. Liu, Y. W. Zhang, L. D. Chen and X. H. Cheng, *J. Appl. Phys.*, 2009, **106**, 073723.
32. M. J. Lee, C. B. Lee, D. Lee, S. R. Lee, M. Chang, J. H. Hur, Y. B. Kim, C. J. Kim, D. H. Seo, S. Seo, U. Chung, I. Yoo and K. Kim, *Nat. Mater.*, 2011, **10**, 625-630.
33. S. Gao, F. Zeng, F. Li, M. J. Wang, H. J. Mao, G. Y. Wang, C. Song and F. Pan, *Nanoscale*, 2015, **7**, 6031-6038.
34. Y. Sharma, P. Misra, S. P. Pavunny and R. S. Katiyar, *Appl. Phys. Lett.*, 2014, **104**, 1-5.
35. S. Gao, C. Song, C. Chen, F. Zeng and F. Pan, *J. Phys. Chem. C,* 2012, **116**, 17955-17959.
36. Y. Takeuchi, G. Yoshizaki and T. Takeuchi, *Nature*, 2004, **430**, 630.
37. J. M. D. Coey, M. Venkatesan, P. Stamenov, C. B. Fitzgerald and L. S. Dorneles, *Phys. Rev. B*, 2005, **72**, 024450.
38. Q. W. Wang, Y. D. Zhu, X. L. Liu, M. Zhao, M. C. Wei, F. Zhang, Y. Zhang, B. L. Sun, and M. Y. Li, *Appl. Phys. Lett.*, 2015, **107**, 063502.

Published on 31 October 2020. Downloaded on 11/1/2020 7:31:47 AM.

Physical Chemistry Chemical Physics Accepted Manuscript

View Article Online
DOI: 10.1039/D0CP03767B

39. G. Y. Chen, G. F. Bi, L. Song, Y. K. Weng, D. F. Pan, Y. C. Li, S. Dong, T. Tang, J. M. Liu, and J. G. Wan, *Appl. Phys. Lett.*, 2016, **109**, 112903.
40. C. Y. Yao, W. Hu, M. Ismail, S. K. Thatikonda, A. Hao, S. He, N. Qin, W. H. Huang and D. H. Bao, *Curr. Appl. Phys.*, 2019, **19**, 1286-1295.
41. Y. X. Luo, D. Y. Zhao, Y. G. Zhao, F. K. Chiang, P. C. Chen, M. H. Guo, N. N. Luo, X. L. Jiang, P. X. Miao, Y. Sun, A.T. Chen, Z. Lin, J. Q. Li, W. H. Duan, J. W. Cai and Y. Y. Wang, *Nanoscale*, 2015, **7**, 642-649.
42. D. Y. Zhao, S. Qiao, Y. X. Luo, A. T. Chen, P. F. Zhang, P. Zheng, Z. Sun, M. H. Guo, F. K. Chiang, J. Wu, J. L. Luo, J. Q. Li, S. Kokado, Y. Y. Wang and Y. G. Zhao, *ACS Appl. Mater. Interfaces*, 2017, **9**, 10835-10846.
43. V. I. Nikolaev and A. M. Shipilin, *Phys. Solid State*, 2003, **45**, 1079-1080.
44. M. Johnson, *Nat. Nanotechnol.*, 2007, **2**, 143-144.
45. T. Ono, Y. Ooka, H. Miyajima and Y. Otani, *Appl. Phys. Lett.*, 1999, **75**, 1622-1624.

Published on 31 October 2020. Downloaded on 11/1/2020 7:31:47 AM.

Physical Chemistry Chemical Physics Accepted Manuscript

View Article Online
DOI: 10.1039/D0CP03767B

Fig. 1 Structural analysis of the Pt/Gd_2O_3/ITO memristor. (a) Schematic memristor structure with measurement configuration. (b) Cross-sectional HRTEM image of the memristor. Inset: the magnified lattice fringe image of one typical Gd_2O_3 crystalline grain. (c) XRD pattern of the as-deposited Gd_2O_3 film on a glass substrate. (d) Conductivity mapping of the as-deposited Gd_2O_3 film obtained by SPM with a read voltage of 0.02 V.

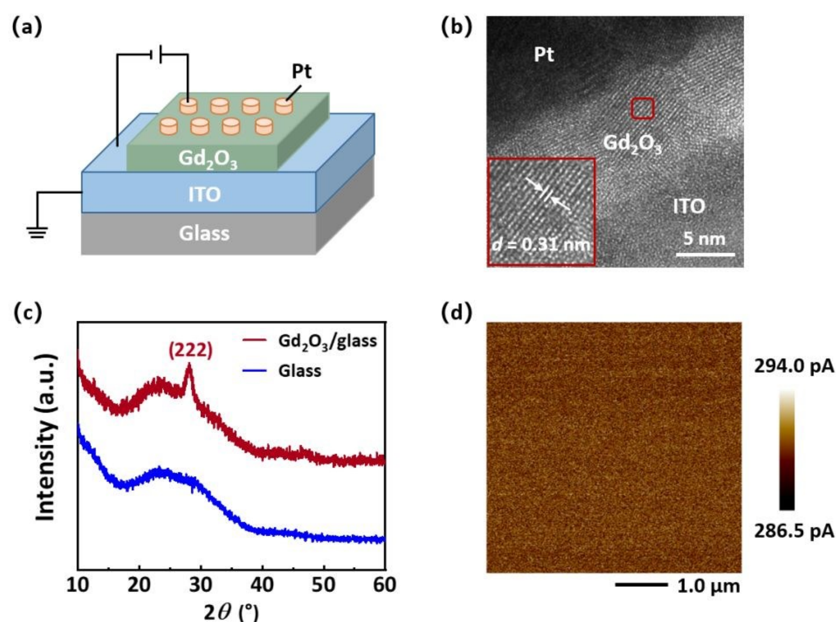

Published on 31 October 2020. Downloaded on 11/1/2020 7:31:47 AM.

Physical Chemistry Chemical Physics Accepted Manuscript

View Article Online
DOI: 10.1039/D0CP03767B

Fig. 2 Resistive switching performance and mechanism of the Pt/Gd_2O_3/ITO memristor. (a) *I*–*V* curves of the first and second resistive switching cycles of a fresh memristor. (b) Operation voltage distributions of the memristor. (c) Data retention properties of the memristor measured with a read voltage of 0.02 V. (d) Temperature-dependent resistance of the memristor in LRS measured with a constant current of 20 μA. (e) Cross-sectional HRTEM analysis of the memristor in LRS. Lattice fringe and fast Fourier transformed images of the CF region and the surrounding Gd_2O_3 region are shown in (e-2, e-3) and (e-4, e-5), respectively.

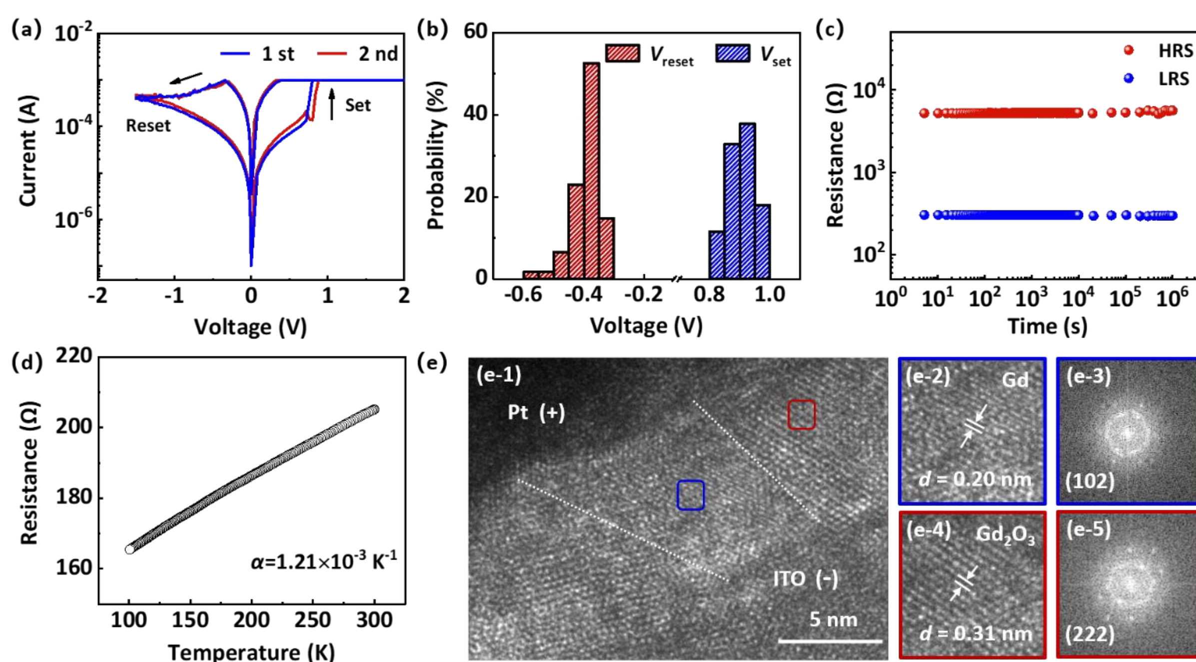

Published on 31 October 2020. Downloaded on 11/1/2020 7:31:47 AM.

Physical Chemistry Chemical Physics Accepted Manuscript

View Article Online
DOI: 10.1039/D0CP03767B

Fig. 3 Magnetism modulation and MR behavior of the Pt/Gd_2O_3/ITO memristor. (a) Sample configuration and magnetic field direction for magnetization measurement. (b) Magnetization characteristics of the sample in various resistance states. (c) Repeatable saturation magnetization modulation of the sample by resistive switching. (d) Sample configuration and magnetic field direction for MR measurement. MR behaviors of the sample in (e) LRS and in (f) HRS were read at 1 μA.

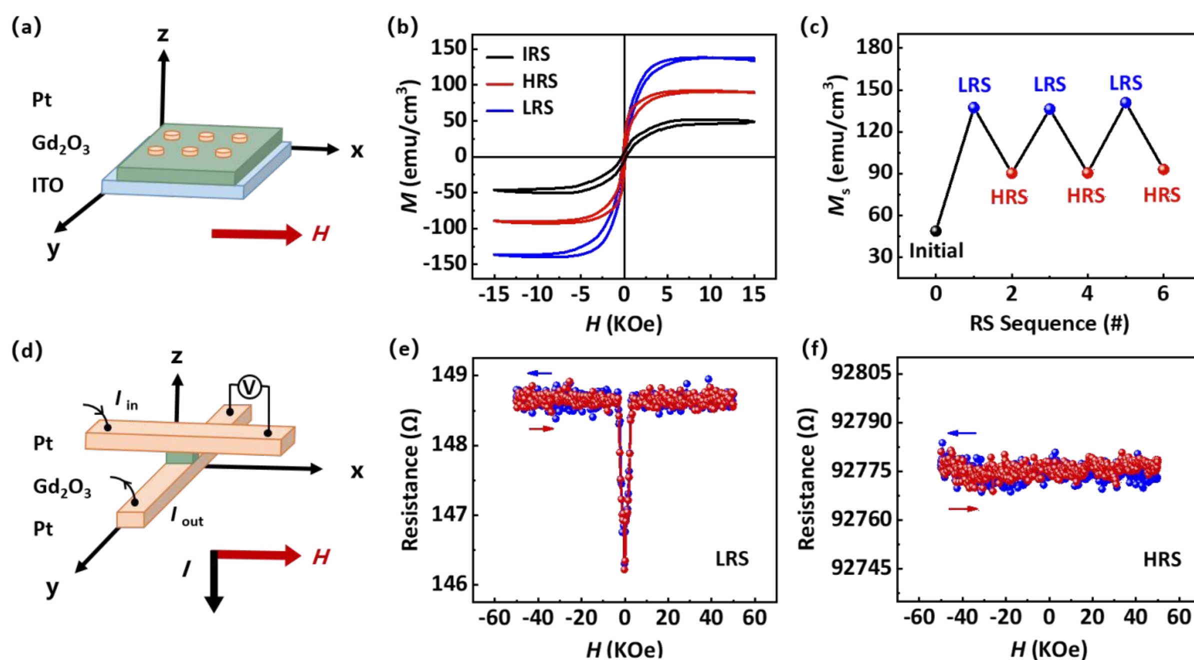

Published on 31 October 2020. Downloaded on 11/1/2020 7:31:47 AM.

Physical Chemistry Chemical Physics Accepted Manuscript

View Article Online
DOI: 10.1039/D0CP03767B

Fig. 4 Conductance quantization of the Pt/Gd_2O_3/ITO memristor. (a) Stepwise evolution of the memristor conductance during reset process. (b) Evolution of the memristor conductance as a function of the stop voltage during reset process. (c) Histogram of the memristor conductance based on 1376 reset traces. (d) Repeatability of the quantized conductance states between $1G_0$ and $10G_0$. (e) Data retention properties of the selected quantized conductance states. All the conductance values in (b-e) were read at 0.02 V.

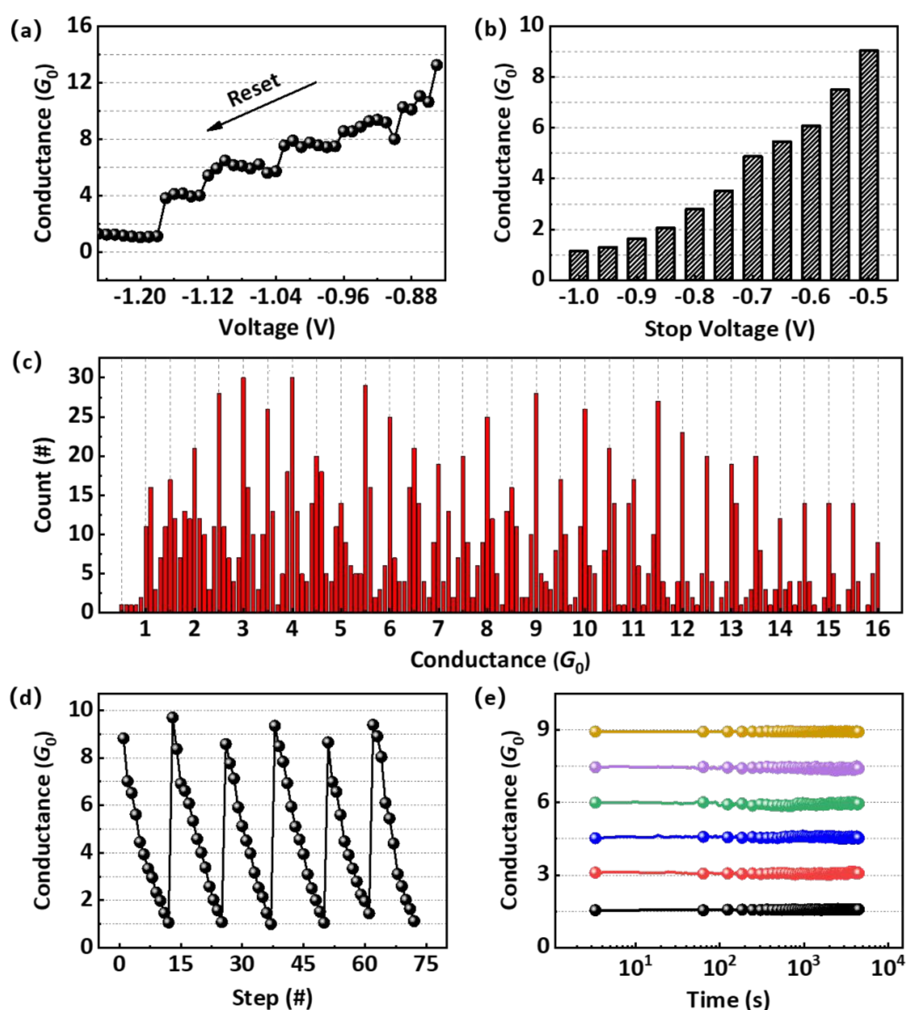

Published on 31 October 2020. Downloaded on 11/1/2020 7:31:47 AM.

Physical Chemistry Chemical Physics Accepted Manuscript